Alpha-linoleic acid (ALA) as a corrosion inhibitor for XC48 steel in H_2SO_4 medium: an experimental and computational study

C. Merimi,[1] K. Zaidi,[1] B. Hammouti,[1,2]* L. Guo,[3,4] S. Kaya,[5] H. Elmsellem,[1] A. Aouniti,[1] M. Bouklah[1] and R. Touzani[1]

[1]*University Mohammed Premier, Faculty of Sciences, Laboratory: Applied Chemistry and Environment (LCAE), Department of chemistry, BP 717, 60000 Oujda, Morocco*
[2]*Centre de Recherche, Ecole des Hautes Etudes d'Ingenierie EHEIO, Oujda, Morocco*
[3]*School of Material and Chemical Engineering, Tongren University, Tongren 554300, PR China*
[4]*School of Oil and Natural Gas Engineering, Southwest Petroleum University, Chengdu 610500, PR China*
[5]*Sivas Cumhuriyet University, Health Services Vocational School, Department of Pharmacy, 58140, Sivas, Turkey*
**E-mail: hammoutib@gmail.com*

Abstract

Iron and steel materials are extensively used in many industries due to low cost and availability. We suggested alpha-linolenic acid (ALA) to slow down the corrosion of XC48 steel in H_2SO_4 solution. We chose ALA because it comprises a carboxylic group and an aliphatic chain containing 17 carbons with three double bonds. This work was conducted by electrochemical measurements (stationary current–voltage curves) and gravimetric measurements (weight loss method) at various temperatures (298–348 K). The findings show that this agent acts as a strong inhibitor in a large concentration range. The inhibition effect is 92% at a concentration of $5 \cdot 10^{-3}$ M. Adsorption and activation parameters were also evaluated. Conceptual Density Functional Theory calculations and the results of the Molecular Dynamic Simulation Approach are in good agreement with the experimental observations.

Received: July 20, 2022. Published: October 10, 2022 doi: 10.17675/2305-6894-2022-11-4-3

Keywords: *alpha-linolenic acid, carbon steel, corrosion, protection, inhibitors, H_2SO_4 solution.*

Introduction

Corrosion attack of steel reinforcement in concrete is a problem of great importance, since the annual costs attributable to corrosion and its consequences amount to several billion dollars in industrialized countries [1]. Corrosion inhibitors are among the most effective solutions to this problem, however, their effectiveness under real conditions remains to be evaluated. The causes of corrosion are multiple and complex and result from chemical and/or physical interactions between the material and its environment. Organic inhibitors

have been widely applied to protect metals from corrosion in many aggressive acidic media. The presence of S, N, O, and P atoms in the molecular structure of an inhibitor have been found to play a great role in corrosion inhibition [2–6]. The effectiveness of these compounds as corrosion inhibitors has been interpreted in terms of molecular structure, molecular size, molecular weight, heteroatoms present, and adsorption tendency. Under certain conditions, the electronic structure of organic inhibitors has a decisive influence on the effectiveness of corrosion inhibition of metals. Inhibitors affect the kinetics of the electrochemical reactions that constitute the corrosion process and thus modify the dissolution of the metal in acids. Existing data show that most organic inhibitors act by adsorption on the metal surface. Numerous studies have been conducted to determine the adsorption of various compounds at the electrode/solution interface [7–10]. Numerous organic compounds have been investigated as corrosion inhibitors. Unfortunately, most of the organic inhibitors used are very expensive and pose health risks. Their toxic properties limit their field of application. The objective is to find cost-effective and non-hazardous inhibitors for the protection of metals against corrosion. The literature dealing with environment-friendly inhibitors has become rich in the last decades [11–14]. Alpha-linolenic acid (ALA) was studied as a non-toxic corrosion inhibitor for carbon steel in acidic H_2SO_4 environments. ALA is a carboxylic acid with a long unbranched aliphatic chain that has both saturated and unsaturated regions. Molecules comprising a carboxylic group and aliphatic chain containing double bonds are used as corrosion inhibitors of iron and steel in aggressive media [15–21]. The objective of this work is to examine the inhibitory action of alpha-linolenic acid (ALA) for the corrosion of carbon steel in 0.5 M H_2SO_4 environments at various temperatures (298–348 K). DFT calculations and MD simulations were also conducted to explain the inhibition process.

Materials and Methods

Preparation of steel samples

The product under review is XC48 carbon steel characterized by the following general composition by weight: C = 0.48%, Mn = 0.66%, Si = 0.27%, Ni = 0.02%, Cr = 0.21%, Mo = 0.02% and Fe = 98.21%. The samples were cut into parallelepiped shapes of 2.0×2.0×0.5 cm and had a total exposed area of 12 cm^2. Electrochemical experiments were performed using a Radiometer analytical instrument (Voltalab-PGZ 100) driven by a computer equipped with Voltamaster 4 software. The electrochemical cell included a mild steel working electrode (WE), a platinum counter electrode (Pt) and a saturated calomel electrode as a reference electrode. The working electrode (WE) was a flat specimen with an exposed area of 1.0 cm^2 embedded in inert resin. The samples were carefully polished with emery papers of various grit ranging from 100 to 2000, cleaned with distilled water and then acetone, dried at room temperature, and then prepared for each corrosion experiment. In this work, alpha-linolenic acid (ALA) was selected as a carbon steel corrosion inhibitor (Figure 1). ALA or Omega-3 fatty acids are called polyunsaturated because their carbon

chain includes several double bonds [22]. The term "Omega-3" comes from the fact that the first double bond in the carbon chain of the acid, counting from the end opposite the carboxyl, is located on the third carbon–carbon bond. ALA was initially dissolved in DMSO with stirring for a few minutes and thereafter added to the acid solutions.

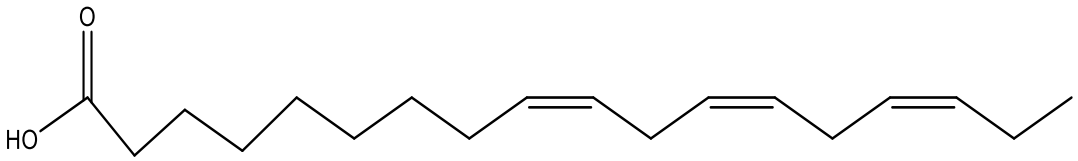

Figure 1. Structure of alpha-linolenic acid (ALA) molecule ($C_{18}H_{30}O_2$).

Corrosive solutions

The acidic corrosive solution 0.5 M H_2SO_4 was obtained by diluting 96% H_2SO_4 in distilled water. Corrosive media solutions containing various amounts of the ALA inhibitor were also prepared.

Experimental procedures

Gravimetric study

Mass loss estimates of the samples were performed in accordance with the conventional approach for evaluating the corrosion behavior of steel. XC48 steel samples were placed into 0.5 M H_2SO_4 solutions at varying concentrations of the inhibitor at 308 K. A comparison solution that contained no inhibitor was also used. After exposure, the XC48 samples were withdrawn from the corrosive medium, washed with purified water, dehydrated with acetone and weighed again to assess the time-dependent efficacy of the corrosion process inhibition at set contact time intervals. For each operating condition, the tests were carried out and the mean value of the loss of weight was reported. For each concentration, the corrosion rate W_{corr} ($g \cdot cm^{-2} \cdot h^{-1}$) and inhibition efficiency (IE%) were determined using the following equation:

$$W = \frac{\Delta m}{St} = \frac{m_1 - m_2}{St} \quad (1)$$

In the given equation, m_1 and m_2 are the mass of XC48 steel sample before and after the immersion in each corrosive solution in mg unit, S (cm^2) is the sample surface area, and t (h) stands for the immersion time in the corrosive medium. The inhibition efficiency (IE%) was calculated as:

$$IE\% = \left(1 - \frac{W_{inh}}{W_0}\right) \cdot 100 \quad (2)$$

where W_0 and W_{inh} are the corrosion rates of XC48 steel in the corrosive medium without and in the presence of the inhibitor, respectively [23–26].

Electrochemical study

The studies were carried out using a three-electrode cell assembly connected to a PGZ100 potentiostat operated by a computer with Voltamaster 4 software. Stationary methods (plotting the polarization curves) and transitory approaches (drawing electrochemical impedance curves on the Nyquist and Bode planes) were used to study the electrochemical processes. The curves were analyzed and plotted Using Zview, Origin and EC-Lab software. Inhibition efficiency (*IE*%) was also determined from the following expression from the Tafel diagram:

$$IE\% = \frac{I_{\text{corr}}^{0} - I_{\text{corr}}}{I_{\text{corr}}^{0}} \tag{3}$$

where I_{corr} and I_{corr}^{0} are the corrosion current densities with and without the inhibitor, respectively.

Theoretical calculation details

DFT calculations

In this work, quantum chemical calculations based on DFT theory were performed using the GGA-BLYP exchange–correlation functionality through the Dmol^3 module of the Material Studio (MS) software developed by BIOVIA. For the computations, the double numeric quality with polarization (DNP) basis set with the COSMO tacit solvent type (water, dielectric constant 78.54) was used. Besides, vibrational analysis was performed to ensure the optimized structures reaching the minimum point on the potential energy surface. The convergence thresholds for energy, maximum force, and maximum atomic displacement were $1\cdot10^{-5}$ Ha, $2\cdot10^{-3}$ Ha·Å^{-1}, and $5\cdot10^{-3}$ Å, respectively. The optimized molecular structure and various quantum chemical descriptors like chemical potential (μ), electronegativity (χ), hardness (η) and softness (σ) in Conceptual Density Functional Theory (CDFT) developed and introduced by Parr were determined [27–30].

$$\mu = -\chi = \left[\frac{\partial E}{\partial N}\right]_{v(r)} = -\left(\frac{I + A}{2}\right) \tag{4}$$

$$\eta = \frac{1}{2}\left[\frac{\partial^2 E}{\partial N^2}\right]_{v(r)} = \frac{I - A}{2} \tag{5}$$

$$\sigma = 1/\eta \tag{6}$$

To calculate the electrophilicity index proposed by Parr [31], the following formula based on absolute hardness and absolute electronegativity was used.

$$\omega \equiv \frac{\chi^2}{2\eta} \tag{7}$$

In the equation given above, E, N, I and A are total electronic energy, total number of the electrons, ground state ionization energy and ground state electron affinity of any chemical system, respectively.

In corrosion inhibition studies, electron donating and electron accepting capabilities are predicted, discussed and compared in the light of useful quantum chemical parameters. Two useful parameters called as electron-donating power and electron-accepting power introduced by Gazquez and coworkers [32] are calculated through the following equations:

$$\omega^{+} = (I + 3A)^2 / (16(I - A)) \tag{8}$$

$$\omega^{-} = (3I + A)^2 / (16(I - A)) \tag{9}$$

The ionization energy (I) and electron affinity (A) of the chemical systems can be approximately estimated from the frontier orbital energies through the relations $I = -E_{\text{HOMO}}$ and $A = -E_{\text{LUMO}}$ as reported by Koopmans [33]. Back-donation energy ($\Delta E_{\text{back-donation}}$) is one of the important parameters of corrosion studies and is calculated based on chemical hardness of any system through the following equation [34–36].

$$\Delta E_{\text{back-donation}} = -\eta / 4 \tag{10}$$

Molecular dynamics (MD) simulation

The MD simulation was carried out employing the Forcite module of MS software. It was performed in a simulation box (2.48 nm×2.48 nm×3.81 nm) with periodic boundary conditions. The box comprises a lower Fe slab and an upper solvent layer (having 800 water molecules and one inhibitor molecule of interest). For the iron substrate, Fe(110) was chosen as the studied surface as it has a densely packed structure and is highly stable; it was simulated with a five-layer Fe slab. In such model, there were 100 Fe atoms in each layer symbolizing a (10×10) unit cell. The whole system was conducted by the Andersen thermostat, NVT canonical ensemble, with a time step of 1.0 fs and simulation time of 1000 ps, using the COMPASS II force field. Non-bond interactions, van der Waals and electrostatic, were set as atom-based simulation approach and Ewald simulation technique, respectively, with a cutoff radius of 1.55 nm. The interaction energy ($E_{\text{interaction}}$) and binding energy (E_{binding}) providing important hints about corrosion inhibition performances of molecules are calculated as [37–39]:

$$E_{\text{interaction}} = E_{\text{total}} - (E_{\text{surface}} + E_{\text{inhibitor}}) \tag{11}$$

$$E_{\text{binding}} = -E_{\text{interaction}} \tag{12}$$

where E_{total} stands for the total energy of the surface and adsorbed inhibitor molecule, E_{surface} represents the energy of the surface without the inhibitor and $E_{\text{inhibitor}}$ is the energy of the adsorbed inhibitor molecule on the surface.

Results and Discussion

Gravimetric study

Table 1. Weight loss parameters for corrosion of XC48 steel in 0.5 M H_2SO_4 at various ALA concentrations at 308 K.

Medium	*T* (K)	*C* (M)	*W* (mg/cm²·h)	θ	*IE* (%)
Blank	298	0.5 M	0.502	–	–
	303		1.569	–	–
	308		1.72	–	–
	318		1.922	–	–
	328		2.963	–	–
	333		8.329	–	–
	348		12.75	–	–
ALA	308	$5 \cdot 10^{-3}$	0.128	0.925	92.5
		$5 \cdot 10^{-4}$	0.157	0.908	90.8
		$5 \cdot 10^{-5}$	0.178	0.896	89.6
		$5 \cdot 10^{-6}$	0.362	0.789	78.9
		$5 \cdot 10^{-7}$	0.392	0.772	77.2

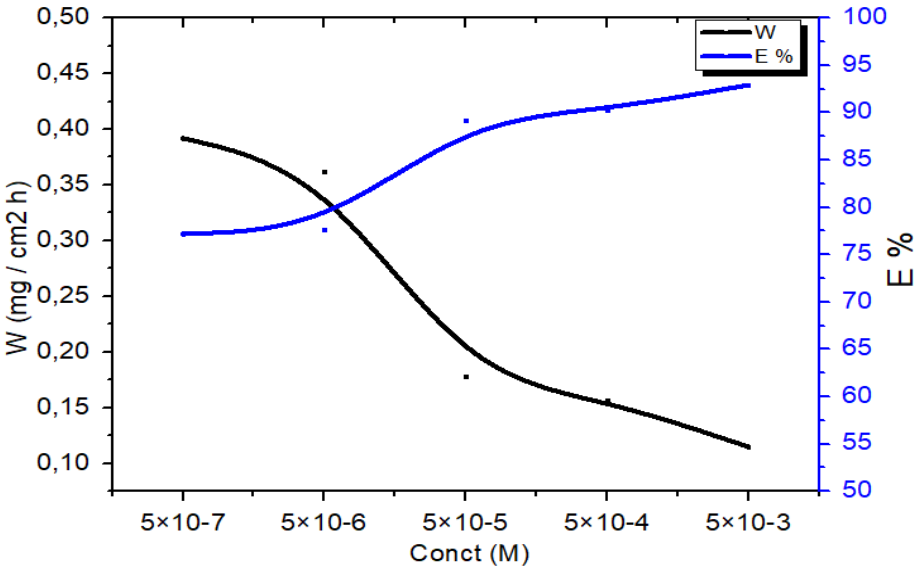

Figure 2. Concentration effect on the corrosion rate and inhibiting efficiency at a temperature of 308 K and 6 h exposure.

Weight loss measurements were carried out in 0.5 M H_2SO_4 in the absence and in the presence of various concentrations of ALA. The values of inhibition efficiency (*IE*%) and corrosion rate (*W*) obtained by the weight loss method at different concentrations of ALA at

308 K are shown in Figure 2. It was observed that the corrosion rate decreased with an increase in inhibitor concentration and temperature. Table 1 indicates that ALA prevents carbon steel corrosion in the H_2SO_4 solution at all the concentrations used, *i.e.*, $5 \cdot 10^{-7}$ to $5 \cdot 10^{-3}$ M. The maximum inhibition efficiency was obtained at a concentration of $5 \cdot 10^{-3}$ M. The improved inhibition performance and reduced corrosion rate may be attributed to increased absorption and increased inhibitor surface distribution on the XC48 carbon steel surface with an increase in concentration [40–42].

Effects of immersion time and concentration

Table 2. Weight loss parameters for the corrosion of XC48 steel in 0.5 M H_2SO_4 at different inhibitor concentrations.

Immersion Time (h)	Corrosion rate W (g·cm^{-2}·h^{-1})					
	C (M)					
	Blank	$5 \cdot 10^{-3}$	$5 \cdot 10^{-4}$	$5 \cdot 10^{-5}$	$5 \cdot 10^{-6}$	$5 \cdot 10^{-7}$
1	2.415	0.086	0.108	0.149	0.187	0.178
2	2.527	0.112	0.133	0.166	0.256	0.228
4	2.622	0.128	0.157	0.178	0.362	0.392
6	2.834	0.253	0.228	0.355	0.572	0.601
8	2.982	0.324	0.564	0.688	0.738	0.688
12	2.955	0.421	0.617	0.763	0.933	0.994
24	3.151	0.622	0.826	1.017	1.233	1.367

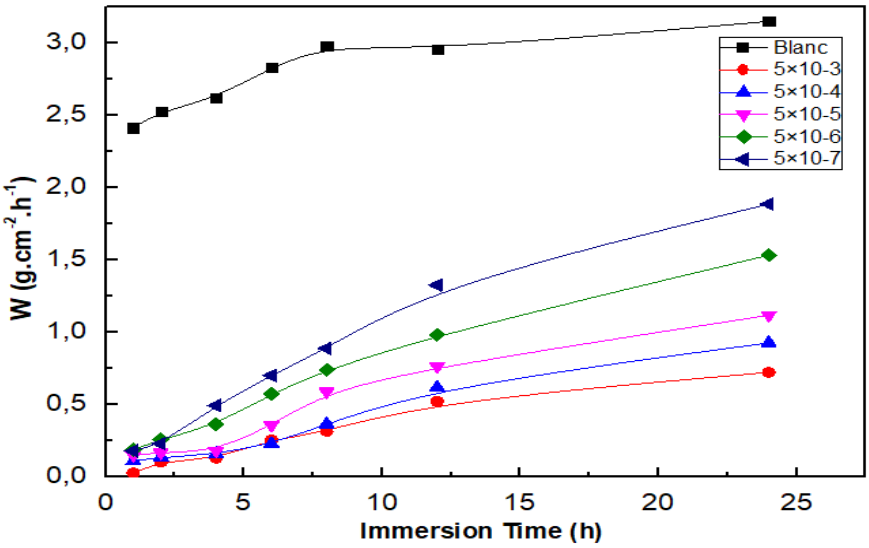

Figure 3. Weight loss – time curves for the corrosion of XC48 steel in 0.5 M H_2SO_4, with and without the inhibitor at different concentrations of alpha-linoleic acid.

We focused on the other effects as a function of time. The results are shown in the table of inhibitory efficacy findings. The graphs shown in Figures 3 and 4 demonstrate the variation in the corrosion rate and inhibition performance of XC48 steel in 0.5 M H_2SO_4 solution in the absence and in the presence of various ALA concentrations at a temperature of 308 K. For this inhibitor, we see that with an increase in the inhibitor concentrations the corrosion rate *W* declines while the protection performance *IE*% increases [43].

Table 1. Inhibitory efficacy results as a function of time.

Immersion Time (h)	*IE* %				
	C (M)				
	$5 \cdot 10^{-3}$	$5 \cdot 10^{-4}$	$5 \cdot 10^{-5}$	$5 \cdot 10^{-6}$	$5 \cdot 10^{-7}$
1	96.431	96.438	95.527	92.256	92.629
2	95.833	94.736	93.431	89.869	88.919
4	95.118	94.012	93.211	86.193	85.049
6	91.072	91.954	87.473	79.816	78.793
8	89.134	81.086	76.928	74.481	76.928
12	85.753	79.120	74.179	68.426	66.362
24	80.260	73.786	67.724	60.869	56.616

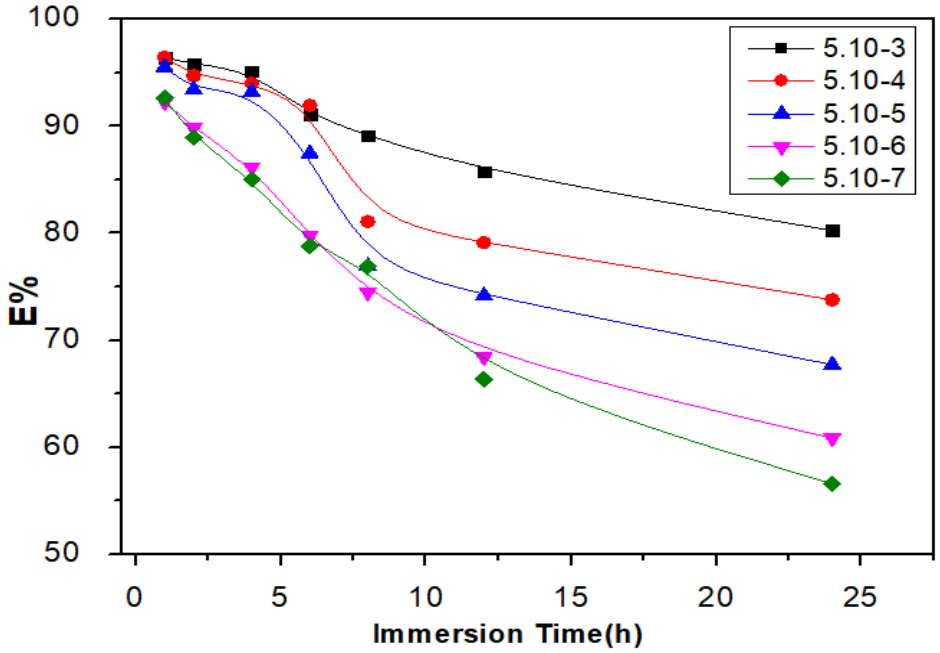

Figure 4. Inhibitive efficiency for corrosion of XC48 steel in 0.5 M H_2SO_4 at different concentrations of alpha-linolenic acid as a function of time.

Temperature and concentration effects

The effect of temperature in the range of 298–348 K on the corrosion rate and inhibition efficiency at different concentrations of ALA was studied by weight loss measurements and the results are given in Table 4.

Table 2. Weight loss and inhibitive efficiency as a function of temperature.

C **(M)**	***T*** **(K)**	***W*** **(mg·cm^{-2}·h^{-1})**	***IE*** **%**
Blank	298	1.562	–
	308	2.622	–
	318	2.744	–
	328	3.927	–
	338	6.459	–
	348	11.871	–
$5\cdot10^{-3}$	298	0.113	92.765
	308	0.137	94.774
	318	0.219	92.018
	328	0.275	92.997
	338	1.066	83.495
	348	4.235	64.324
$5\cdot10^{-4}$	298	0.128	91.805
	308	0.157	94.012
	318	0.334	91.494
	328	0.764	88.171
	338	2.012	83.051
	348	6.528	45.008
$5\cdot10^{-5}$	298	0.133	91.485
	308	0.178	93.211
	318	0.420	84.693
	328	1.361	65.342
	338	2.855	55.798
	348	8.0 67	32.044

***C* (M)**	***T* (K)**	***W* (mg·cm^{-2}·h^{-1})**	***IE*%**
$5 \cdot 10^{-6}$	298	0.256	83.611
	308	0.362	86.193
	318	0.554	79.81
	328	1.806	54.01
	338	3.280	49.218
	348	8.825	25.659
$5 \cdot 10^{-7}$	298	0.664	57.49
	308	0.893	65.94
	318	1.523	44.497
	328	2.402	38.833
	338	4.131	36.042
	348	10.227	13.848

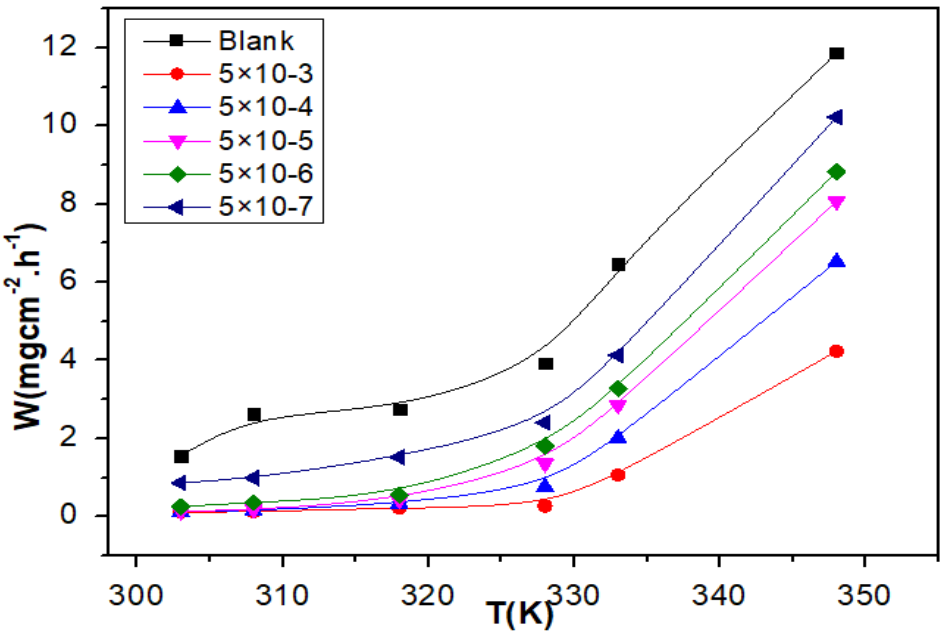

Figure 5. Corrosion rate determined from weight loss as a function of temperature.

Weight loss measurements were performed for 2 hours to 24 hours of immersion in the temperature range of 298–348 K, in the absence and in the presence of $5 \cdot 10^{-3}$ M inhibitor, in order to examine the effect of time on the corrosion inhibition property of the inhibitor. The parameters obtained that are listed in Table 4 clearly indicate an increase in the corrosion rate (W_{corr}) as the temperature increases (Figure 5). It can also be noted that the efficacy of inhibition (Figure 6) depends on time and decreases as the temperature rises from 298 to

328 K. This is due to a shift of the adsorbent/desorption equilibrium towards the desorption of the inhibitor and thus to a decrease of the degree of surface coverage [44].

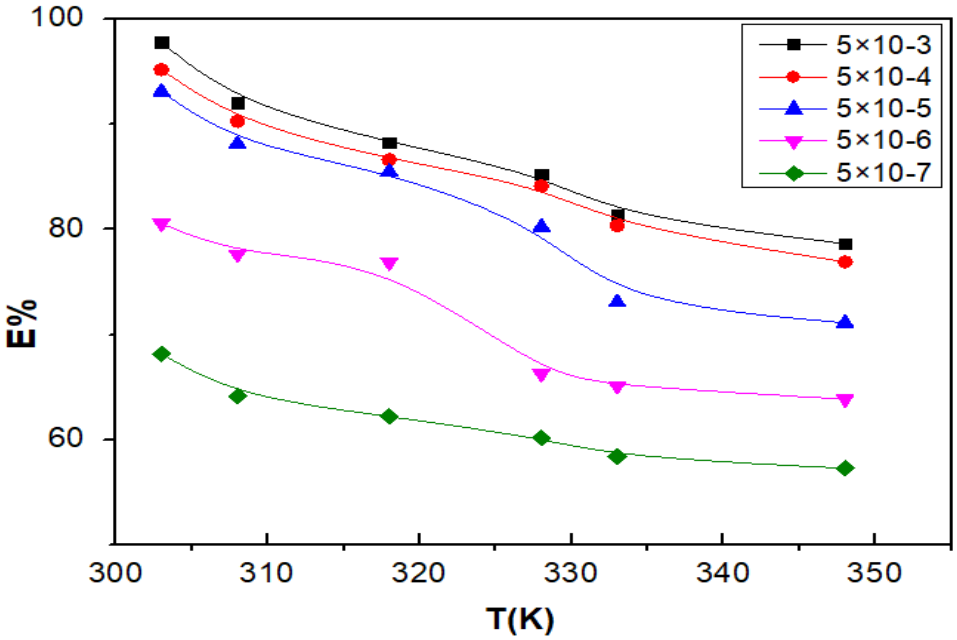

Figure 6. Effect of temperature and inhibitor concentration on inhibition efficiency.

Kinetic parameters of activation

The influence of temperature on the kinetic process of corrosion in the free acid and in the presence of an adsorbed inhibitor provides more information on the electrochemical behaviour of metallic materials in aggressive media. The corrosion reaction of carbon steel in H_2SO_4 media is temperature dependent. The dependence of the rate constant K of chemical reactions on temperature T is expressed by the Arrhenius law:

$$K = A\exp(-E_a / RT) \tag{13}$$

Van't Hoff first suggested equation (13) in 1884; Arrhenius provided a physical justification and interpretation for it five years later in 1889. The Arrhenius law may be presented as a straight line of the logarithm of the corrosion rate (W) *vs.* $1/T$ as pointed out [45] according to the following relation:

$$\ln W = -\frac{E_a}{RT} + \ln A \tag{14}$$

The plots of linear regression between $\ln W$ and $1000/T$ are shown in Figure 7. Table 5 collects the calculated activation energies, E_a, and pre-exponential factors at different inhibitor concentrations. The change in the values of the apparent activation energies may be explained by a modification of the mechanism of the corrosion process in the presence of adsorbed inhibitor molecules. In our study, E_a increases with increasing ALA concentration.

This type of inhibitor retards corrosion at ordinary temperatures but inhibition is diminished at elevated temperature. The corrosion rate increases with temperature, and E_a and A may vary with temperature, according to the Arrhenius law (Eq. 14). The A and E_a values obtained seem to increase continuously with the inhibitor concentration.

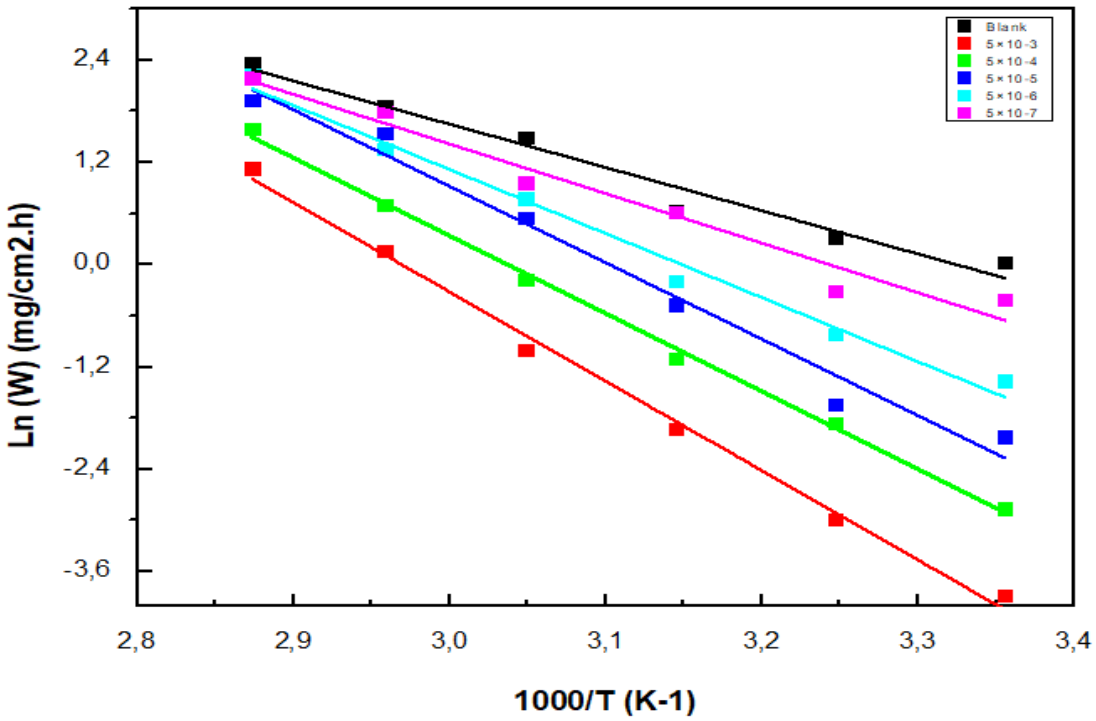

Figure 7. Arrhenius plots of carbon steel XC48 in 0.5 M H_2SO_4 with and without different concentrations of ALA.

Table 5. Some activation parameters of ALA at different concentrations.

C (M)	Pre-exponential factor ($mg \cdot cm^{-2} h^{-1}$)	Linear regression coefficient	E_a ($kJ \cdot mol^{-1}$)	ΔH_a^0 ($kJ \cdot mol^{-1}$)	ΔS_a^0 ($J \cdot mol^{-1} \cdot K^{-1}$)	$E_a - \Delta H_a^0$ ($kJ \cdot mol^{-1}$)
Blank	$8.62 \cdot 10^6$	0.96014	42.15	39.6991	149.56	2.45
$5 \cdot 10^{-3}$	$2.08 \cdot 10^{13}$	0.99389	87.13	85.0927	77.22	2.45
$5 \cdot 10^{-4}$	$1.77 \cdot 10^{11}$	0.99683	75.90	73.5595	44.47	2.34
$5 \cdot 10^{-5}$	$1.60 \cdot 10^{11}$	0.99745	74.49	71.8450	27.17	2.64
$5 \cdot 10^{-6}$	$4.51 \cdot 10^9$	0.98337	62.43	60.0736	58.93	2.36
$5 \cdot 10^{-7}$	$2.22 \cdot 10^7$	0.95637	48.38	45.7710	105.49	2.61

Other kinetic data (enthalpy and entropy of corrosion process) are accessible using an alternative formulation of the Arrhenius equation [46]:

$$W = \frac{RT}{Nh}\exp\left(\frac{\Delta S^0}{R}\right)\exp\left(-\frac{\Delta H^0}{R}\right) \quad (15)$$

where h is Plank's constant, N is Avogadro's number, ΔS_a^0 and ΔH_a^0 are the entropy and enthalpy of activation, respectively. Plots of $\ln W/T$ *vs*. inverse temperature show straight lines with a slope equal to $(-\Delta H_a^0/R)$ and an intercept of $(\ln R/Nh + \Delta S_a^0/R)$. The values of ΔH_a^0 and ΔS_a^0 are also presented in Table 5.

Inspection of the kinetic data shown in Table 5 indicates that all the corrosion process parameters increase with the concentration of the inhibitor. The positive sign of enthalpy (ΔH_a^0) demonstrates the endothermic nature of the metal dissolution process, as postulated in the literature. The entropy of activation ΔS_a^0 in the absence of inhibitors is positive and this value increases positively with the ALA concentration. The increase in ΔS_a^0 implies that there is an increase in disorder from reactants to the activated complex [47].

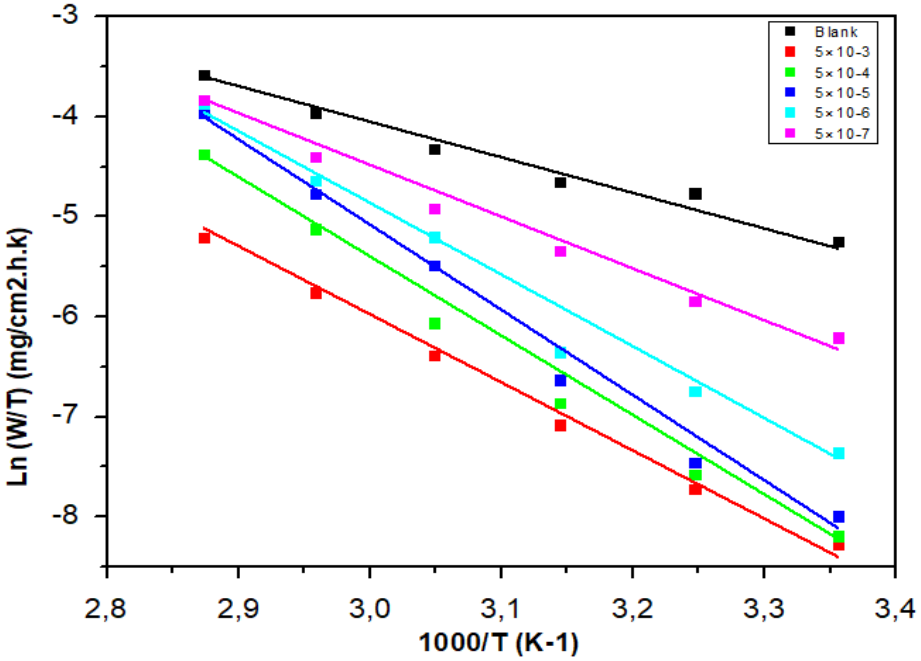

Figure 8. Relationship between $\ln(W/T)$ and T^{-1} for different concentrations of ALA.

The rise of E_a and ΔH_a^0 with an increase in ALA concentration (Figure 8) shows that the energy barrier of the corrosion reaction increases with the concentration of the inhibitor. The higher activation energy in the presence of the inhibitor further confirms the process of physisorption suggested. Unchanged or lower values of E_a in inhibited systems compared to the blank are indicative of the chemisorption mechanism, while higher values of E_a suggest the physical adsorption mechanism. This type of inhibitors retards the corrosion [48].

As described by Bockris & Reddy, 1970 as well as Antropov, 1972, adsorbed hydrogen atoms upon reduction first desorb from the catalyst surface and then recombine into molecules [49, 50]:

$$H_{ads} \rightarrow H \quad (16)$$

The slowest of the following processes at the metal interface control the hydrogen overvoltage and the reaction mechanism: (1) discharge reaction; (2) the transport of the electroactive species to the electrode interface; (3) desorption of hydrogen from the metal surface including catalytic desorption, electrochemical hydrogen desorption, or emission; and (4) gaseous hydrogen formation. This assumption can be interpreted by the known thermodynamic relationship between E_a and ΔH_a^0:

$$E_a - \Delta H_a^0 = RT \quad (17)$$

The difference obtained by Equation 17 is around 2.48 kJ/mol indicating that the activation on the steel surface occurs only by a monoatomic process [51–54].

Adsorption isotherm and thermodynamic parameters

Different isotherms will determine the form of interactions between the alpha-linolenic acid molecules and the metal surface: Langmuir, Temkin, Frumkin. The most suitable isotherm was determined from the linear correlation coefficient (R^2) values. The Langmuir adsorption isotherm proved to be the most appropriate. It is related to the inhibitor concentration by the interaction according to this isotherm.

$$\frac{C_{inh}}{\theta} = \frac{1}{K_{ads}} + C_{inh} \quad (18)$$

where C_{inh} is the concentration of the inhibitor and θ is the degree of surface coverage where K_{ads} is the equilibrium constant of the adsorption process. The Langmuir isotherm followed a linear relation with $R^2 > 0.999$ in our case (Figure 9). These results indicate that the adsorption obeyed the Langmuir isotherm [55].

Table 6. Thermodynamic parameters of the adsorption of ALA on XC48 carbon steel in H_2SO_4 at 308 K.

***T* (K)**	***R*²**	***K*ads**	**Δ*G*ads, kJ·mol⁻¹**
298	0.9998	592066.31	–42.88
308	0.9999	310939.47	–42.673
318	0.9988	156685.91	–42.24
328	0.9999	90985.41	–42.09
338	0.9999	45499.41	–41.42
348	0.9997	28383.71	–41.28

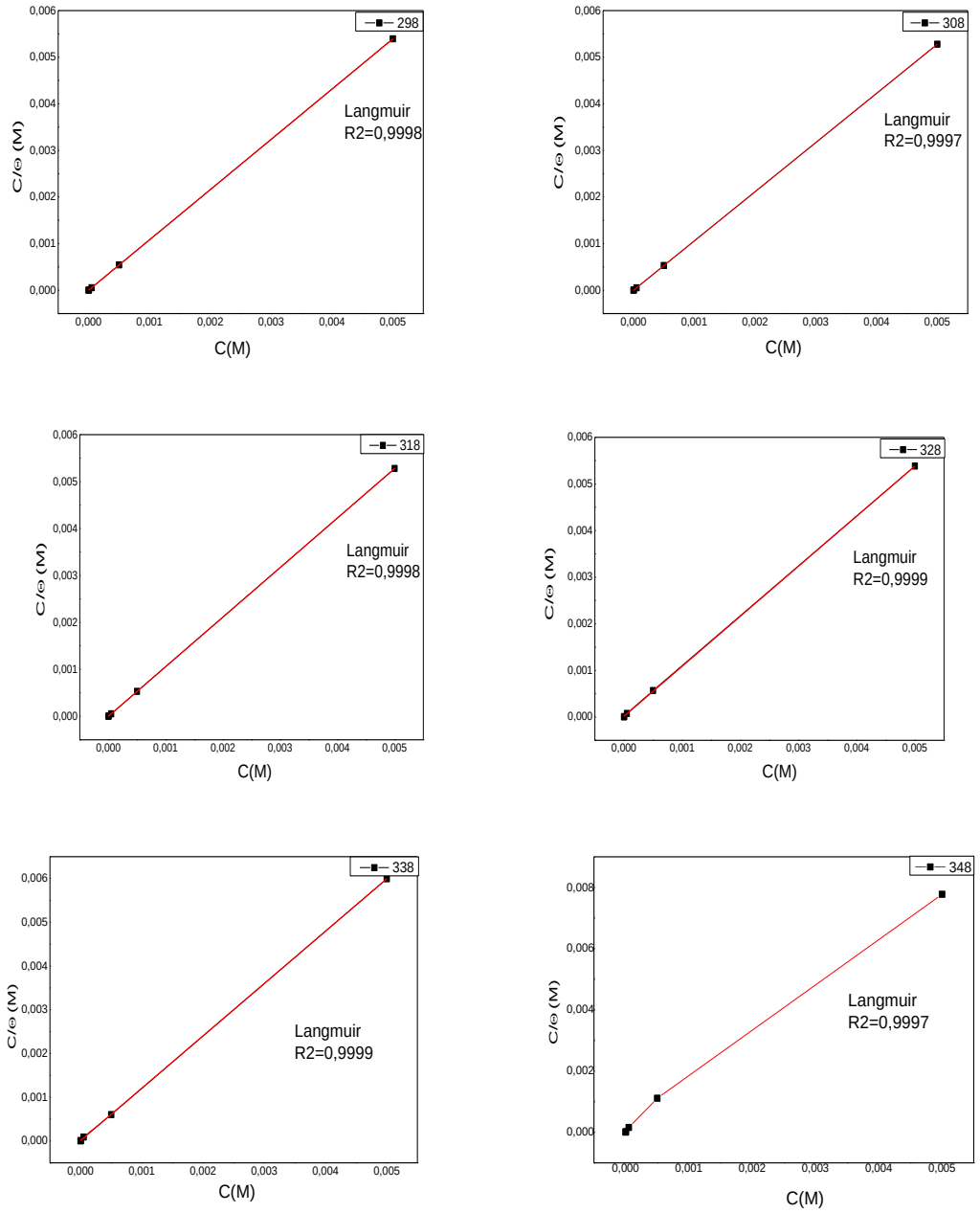

Figure 9. Langmuir isotherm adsorption model of alpha-linolenic acid on the mild steel surface in 0.5M H_2SO_4 at different temperatures.

In addition, from the K_{ads} calculated from the intercept of the straight lines, the free adsorption energy ΔG^0_{ads} may be obtained according to the equation [56]:

$$\Delta G^0_{ads} = -RT \ln(55.5 K_{ads}) \quad (19)$$

where R is the gas constant, T the absolute temperature and 55.5 is the molar water concentration in the bulk solution. The ΔG^0_{ads} value is –42.67 kJ·mol^{-1} at 308 K. The adsorption is usually assumed to be the physisorption at ΔG^0_{ads} values of about –20 kJ·mol^{-1}

or less negative. For those around –40 kJ·mol^{-1} or higher, the adsorption is regarded as chemisorption [57]. The values of ΔG^0_{ads} show that the adsorption of ALA at the XC48 steel surface in the current sample is chemisorption.

The high adsorption potential of this inhibitor on carbon steel XC48 in 0.5 M H_2SO_4 on the surface of this carbon steel is demonstrated by the high benefit of the constant K_{ads} as it facilitates a greater recovery of the metal surface and provides a more productive protection against corrosion. On the other hand, the negative value demonstrated the spontaneous adsorption of ALA molecules on the surface of carbon steel. In addition, this value provides proof of the inhibitor's charge sharing or transition to the charged carbon steel surface XC48 (chemisorption). Finally, we find that the inhibitory function of the drug is enhanced by high values of K_{ads} and ΔG^0_{ads}.

Tafel potentiodynamic polarization curves

In the potentiostatic method, the electrode potential is stabilized for 30 min before proceeding to the measurements of the current/potential curves. Figure 10 demonstrates the potentiodynamic polarization curves of carbon steel XC48 after immersion in 0.5 M H_2SO_4 corrosive solution in the absence and in the presence of different concentrations of ALA at 308 K. The electrochemical parameters extracted by extrapolation from the Tafel lines, such as E_{corr}, I_{corr} and *IE*%, are shown in Table 7 from which it is clear that injection of the inhibitor into a solution of 0.5 M H_2SO_4 results in a minor displacement of the corrosion potential with respect to the control solution, namely, less than 37 mV. These values are smaller than the ±85 mV E_{corr} change value normally taken as a guide for an inhibitor to be classified as anodic or catholic, so the molecule of alpha-linolenic acid can be assumed to act as a mixed form inhibitor [58].

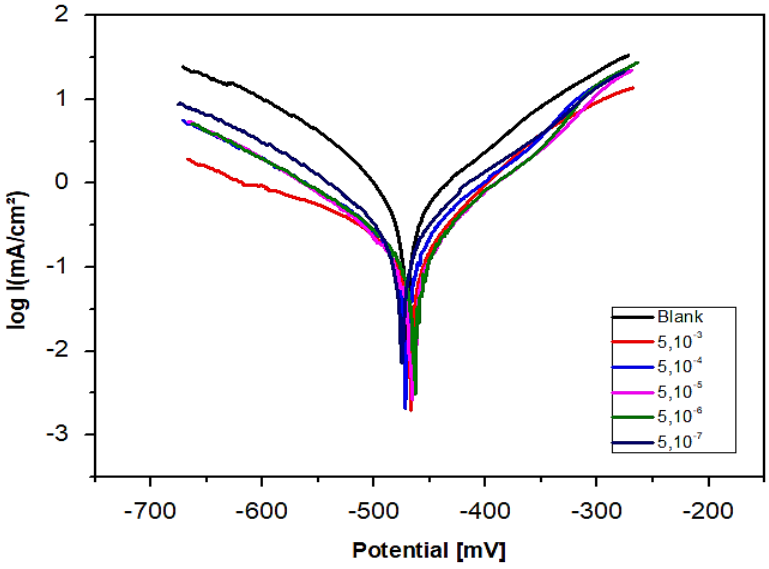

Figure 10. Polarization curves of carbon steel XC48 in 0.5 M H_2SO_4 in the presence and absence of different concentrations of the inhibitor.

Table 7. The electrochemical parameters of mild steel in 0.5 M H_2SO_4 solution without and with different concentrations of the inhibitor at 308 K.

Inhibitor	C (M)	$-E_{corr}$ (mV SCE)	I_{corr} (mA·cm^{-2})	η_{Tafel} (%)
None	0.5	468.9	0.75	–
	$5\cdot10^{-7}$	466.3	0.51	32.27
	$5\cdot10^{-6}$	471.7	0.42	44
ALA	$5\cdot10^{-5}$	463.8	0.31	58.66
	$5\cdot10^{-4}$	460.8	0.098	88.13
	$5\cdot10^{-3}$	472.8	0.061	92.01

Electrochemical impedance spectroscopy was also employed to test the corrosion inhibition efficacy of the inhibitor on XC48 carbon steel (EIS). The spectra obtained for carbon steel in 0.5 M H_2SO_4 in the absence and in the presence of various ALA concentrations at open circuit potential are shown in Figure 11 as Nyquist diagrams. The diagrams all depict basic semicircles, the diameter of which is proportional to the inhibitor concentration. The fact that certain active molecules are adsorbed on the surface of carbon steel and form a protective layer can be clarified. Considering the electrochemical impedance diagrams, we can conclude that there is only one phenomenon that can be explained by the charge transfer process between the XC48 steel and the solution. Moreover, the single semicircle presented in the Nyquist diagrams of all solutions proves that the addition of the product does not modify the dissolution mechanism of the XC48 steel but that the resistance of the carbon steel increases compared to the control solution.

Electrochemical impedance spectroscopy (EIS) studies

The impedance measurements were performed on the Nyquist diagrams. These calculations made it possible to understand certain reaction pathways in elementary systems (charge transfer, diffusion and adsorption). The addition of organic compounds to the corrosive solution resulted in an enhancement in the diameter of the depressed semi-circular shape in the Nyquist diagrams. Furthermore, it increased with increasing inhibitor concentration. These details demonstrate the adsorption on the metal surface of the inhibitor molecules. In the presence of various inhibitor concentrations in the aggressive solution, analysis of Nyquist diagrams (Figure 11) and representative Bode diagrams for carbon steel in H_2SO_4 0.5 M shows a shift in the shape and size of the impedance diagrams, in which a depressed semicircle was found in the high frequency region of the spectrum. The increase in the semicircle size with an increase in inhibitor concentration means that for all the concentrations tested, the influence of the inhibitor also increases, as seen in Figure 11 [59]. The following figure shows the Nyquist diagram in the presence of ALA. The existence of a single capacitive loop indicates that corrosion of carbon steel is largely regulated by a

charge transfer mechanism and the corrosion process remains intact, as the loops have the same shape.

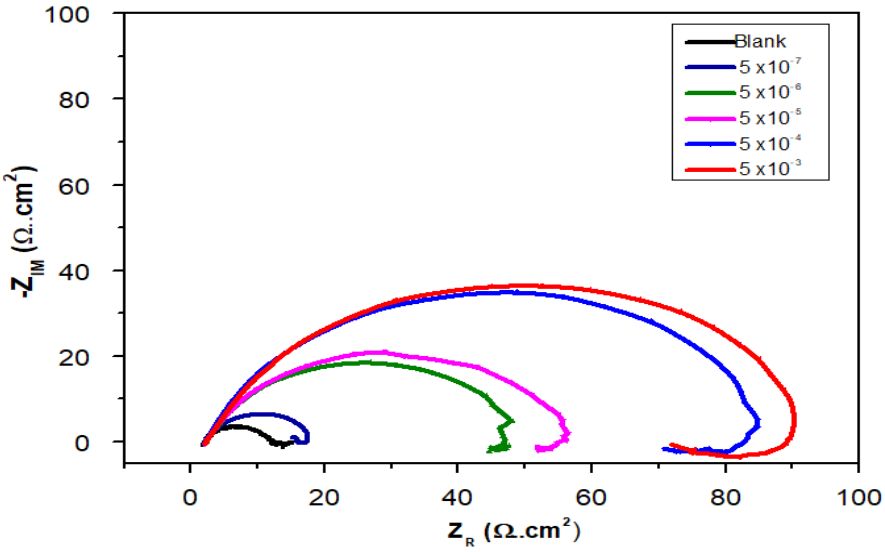

Figure 11. Nyquist diagram of XC48 carbon steel in 0.5 M H_2SO_4 in the absence and presence of different concentrations of ALA at 308 K.

The Bode diagram map, which corresponds to Log $|Z|$ as a function of Log(f), helps one to validate the results obtained from the Nyquist diagram. In addition, more detail is given on the phenomenon taking place at the metal–electrolyte interface, the resistance of the electrolyte that could not be observed in the Nyquist diagram is visualized and specifically visualized. Figure 12 illustrates the Bode diagram map in the absence and presence of ALA in 0.5 M H_2SO_4 medium at 308 K.

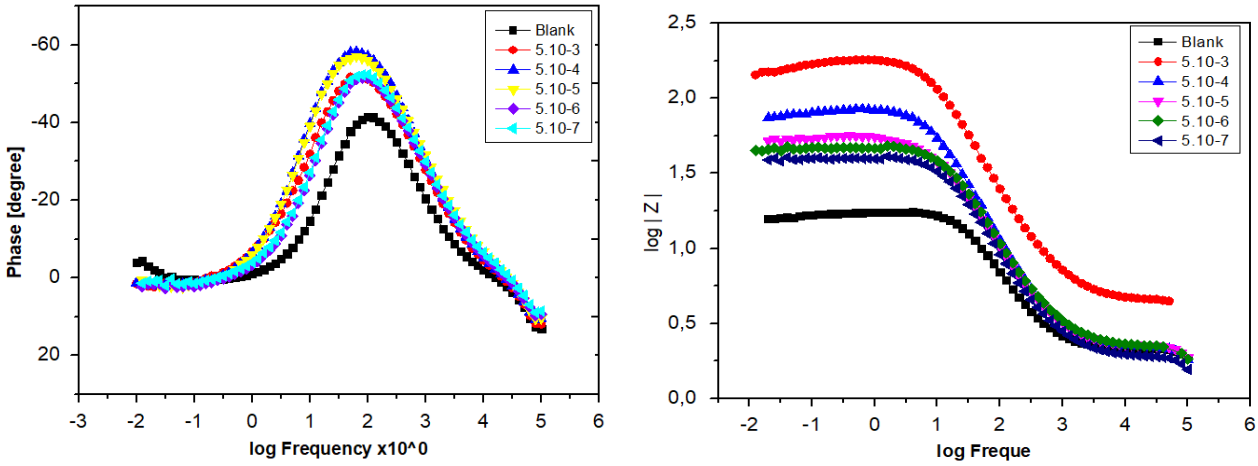

Figure 12. The Bode and phase angle plots for carbon steel in 0.5 M H_2SO_4 in the absence and presence of different concentrations of inhibitors at 308 K at an immersion time of 30 min.

In general, the capacitive layer loop is connected with the phase of charge transfer and the double electric layer. The inclusion of various concentrations of the compounds tested does not alter the semicircle shape. This ensures that the presence of the inhibitor does not modify the corrosion reaction process, but prevents corrosion by increasing the surface coverage of the adsorbed inhibitor film [60]. The Bode phase angle curves clearly demonstrate that the overall phase angle increases with increasing concentration of the tested inhibitor, which indicates that due to the adsorption of molecules on the metal surface at higher concentrations, the compound tested has strong inhibitory activity [61]. The effect of the inhibitor on the corrosion mechanism at the steel/acidic medium interface illustrates this result.

Theoretical Considerations

DFT calculations

The ALA inhibitor's optimized geometry and chemical behavior characteristics are seen in Figure 13. The HOMO regions are predominantly spread over three unsaturated double bonds, while the LUMO regions are spread over the carboxyl group. The electrostatic potential (ESP) distribution can be viewed as a beneficial output from the DFT calculations where it portrays a graphical means where electrophilic and nucleophilic sites of the molecules can be identified. The red area represents nucleophilicity while the blue area signifies electrophilicity. We can see that the red regions are mainly concentrated on oxygen atoms and unsaturated bonds, and these positions are more likely to form covalent bonds with Fe 3d orbitals. Figure 13 also displays the solvated COSMO-cavity for the ALA inhibitor, and as described in the sigma-profile, there are many overlapping areas between the ALA and H_2O molecule, indicating its hydrophilic nature or excellent water solubility.

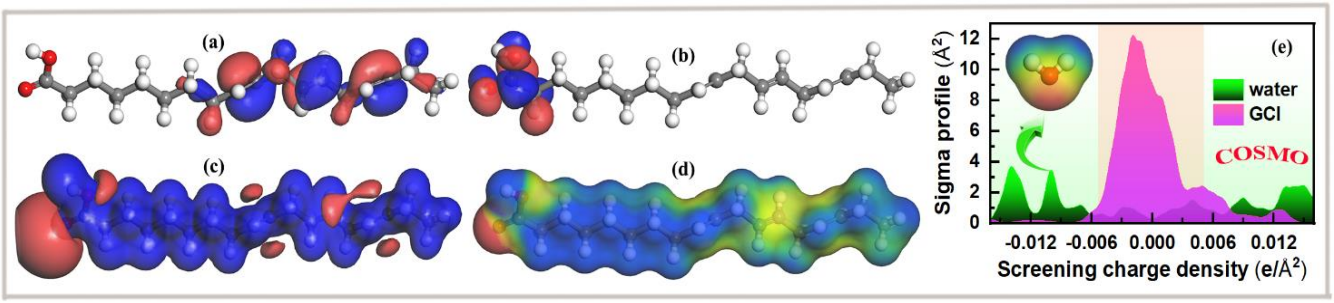

Figure 13. (a) HOMO, (b) LUMO, (c) ESP distribution, (d) COSMO-cavity, and sigma-profile for ALA inhibitor.

Chemical hardness [62, 63] represents the resistance of any chemical system against polarization. For that reason, there is an inverse relationship between the hardness and polarizability parameters. In the light of Hard and Soft Acid-Base Principle, Lewis acids and bases are classified as hard and soft. It should be noted that soft chemical systems with higher polarizability are effective corrosion inhibitors. The Maximum Hardness Principle [64] is

another electronic structure principle about the hardness concept. This principle states that "There seems to be a rule of nature that molecules arrange themselves so as to be as hard as possible." Actually, MHP emphasizes the powerful relationship between hardness and chemical stability. The Minimum Electrophilicity Principle was introduced by Chattaraj *et al*. [65] considering the hardness maximization in stable systems. The Minimum Electrophilicity Principle [66] states that in a stable state, electrophilicity is minimized. The quantum chemical parameters calculated for the studied inhibitor molecule are presented in Table 8. In the present paper, to calculate the number of electrons transferred from the inhibitor molecule to the metal surface, we used the following formula derived in the light of Sanderson's Electronegativity Equalization Principle [67].

$$\Delta N = \frac{\phi_{Fe} - \chi_{inh}}{2(\eta_{Fe} + \eta_{inh})} \quad (20)$$

where in a theoretical value of work-function $\phi_{Fe} = 4.82$ eV [68] was used for the iron surface, η_{inh} represents the hardness of the inhibitor, and η_{Fe} was set to 0 assuming $I = A$ for the bulk metal. When $\Delta N > 0$, the inhibitor molecule transfers its own electrons to the metal and *vice versa* if $\Delta N < 0$. The positive ΔN value (0.329) shown in Table 8 suggest that ALA has the ability to donate electrons to the carbon steel surface. Moreover, it is generally acknowledged that a high dipole moment (μ) exerts a significant effect on the dielectric properties of the electric double layer and enhances the adsorption on the metal surface. The dipole moment value obtained (2.473 Debye) explains well its excellent corrosion inhibition performance. An effective corrosion inhibitor should have higher electron-donating power and ΔN values. If so, one can say that the data presented in the related table support the high inhibition performance obtained *via* experimental procedures.

Table 8. Quantum chemical parameters for ALA at GGA/BLYP/DNP/COSMO level.

Inhibitor	***I* (eV)**	***A* (eV)**	**η (eV)**	**χ (eV)**	**ω (eV)**	**ω⁻ (eV)**	**ω⁺ (eV)**	**μ (D)**	**Δ*N***
ALA	5.578	1.136	2.221	3.357	5.578	4.493	1.136	2.473	0.329

MD simulation

The interaction between the ALA inhibitor and the steel surface was studied by MD simulations. The whole investigated system reached equilibrium until both the temperature as well as energy were balanced. Figure 14a displays the most stable adsorption configurations (top and side views) of ALA on Fe(110) surface. Obviously, the inhibitor molecule tends to be adsorbed on Fe(110) surface in parallel mode to obtain the maximum coverage. From the density field map of ALA on iron substrate (Figure 14b), we can observe that a dense and hydrophobic barrier can be formed to protect steel from corrosion. Figure 14c shows the relative concentration distribution of ALA during the MD process, demonstrating that the highest relative concentration of the inhibitor was near the surface (approximately 2.998 Å). Generally, the radial distribution function (RDF), $g(r)$, illustrates

the length of the link. The peak between 1 and 3.5 Å was attributed to chemisorption, while physisorption was connected with peaks larger than 3.5 Å. The radial distribution function of the centroid of the inhibitor is described in Figure 13d, and clearly the bond length of the Fe (surface)–inhibitor (2.531 Å) is less than 3.5 Å, which manifests that chemisorption is dominant in the investigated adsorption system. Generally, a more negative value of E_{ads} suggests a larger adsorption strength between an inhibitor molecule and the metal surface. The adsorption energies in this work were calculated from the average adsorption energy of the equilibrium configurations obtained. The E_{ads} value obtained is –426.9 kJ/mol for the ALA inhibitor. This negative value indicates the stability of the adsorptive system and spontaneous adsorption can be expected. Overall, our theoretical results account for the experimental findings satisfactorily.

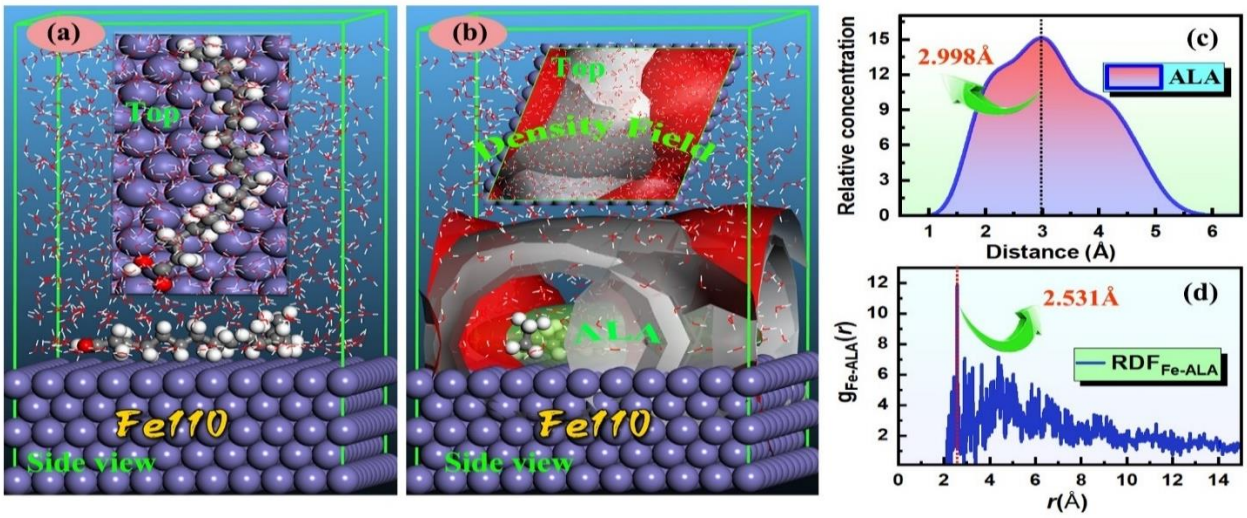

Figure 14. (a) Equilibrium configuration, (b) density field distribution, (c) relative concentration, and (d) RDF plots for the ALA/Fe(110) system.

Conclusion

Weight loss and electrochemical measurements revealed that ALA in H_2SO_4 medium can be considered as a good inhibitor against corrosion of XC48 steel. The active molecules of the inhibitor behave as a mixed inhibitor and adsorbing on the steel surface according to the Langmuir isotherm model. The measured thermal parameters show that the adsorption mechanism is random and exothermic. The surface analysis technique confirmed the electrochemical results and the adsorption of the inhibitor on the surface of XC48 steel. The calculated quantum chemical parameters and adsorption energies are in good agreement with the experiments performed.

Acknowledgements

This work was partially sponsored by the Guizhou Provincial Science and Technology Project (QKHPTRC[2021]5643) and the China Postdoctoral Science Foundation (2022M710117).

References

1. D. Donald, *Electrochemical corrosion testing*, ASTM Publication, Philadelphia, 1981, 110.
2. S. Erdoğan, Z.S. Safi, S. Kaya, D.O. Işın, L. Guo and C.A. Kaya, Computational study on corrosion inhibition performances of novel quinoline derivatives against the corrosion of iron, *J. Mol. Struct*., 2017, **1134**, 751–761. doi: 10.1016/j.molstruc.2017.01.037
3. S.A. Abd El-Maksoud and A.S. Fouda, Some Pyridine Derivatives as Corrosion Inhibitors for Carbon Steel in Acidic Medium, *Mater. Chem. Phys*., 2005, **93**, 84–90. doi: 10.1016/j.matchemphys.2005.02.020
4. S.A.E. Wanees and E.E. Abd El Aal, *N*-Phenylcinnamimide and some of its derivatives as inhibitors for corrosion of lead in HCl solutions, *Corros. Sci*., 2010, **52**, 338–344. doi: 10.1016/j.corsci.2009.09.022
5. H. Rahmani, F. El-Hajjaji, A. El Hallaoui, M. Taleb, Z. Rais, M. El Azzouzi, B. Labriti, K. Ismaily Alaoui and B. Hammouti, Experimental, quantum chemical studies of oxazole derivatives as corrosion inhibitors on mild steel in molar hydrochloric acid medium, *Int. J. Corros. Scale Inhib*., 2018, **7**, no. 4, 509–527. doi: 10.17675/2305-6894-2018-7-4-3
6. B. Hammouti, A. Aouniti, M. Taleb, M. Brighli and S. Kertit, L-Methionine methyl ester hydrochlorid as corrosion inhibitor of iron in 1 M HCl, *Corrosion*, 1995, **51**, no. 6, 411–416.
7. L. Guo, S. Kaya, I.B. Obot, X. Zheng and Y. Qiang, Toward understanding the anticorrosive mechanism of some thiourea derivatives for carbon steel corrosion: A combined DFT and molecular dynamics investigation, *J. Colloid Interface Sci*., 2017, **506**, 478–485. doi: 10.1016/j.jcis.2017.07.082
8. H. Al-sharabi, K. Bouiti, F. Bouhlal, N. Labjar, G. Amine Benabdellah, A. Dahrouch, L. Hermouch, S. Kaya, B. El Ibrahimi, M. El Mahi, E.M. Lotfi, B. El Otmani and S. El Hajjaji, Anti-corrosive properties of Catha Edulis leaves extract on C38 steel in 1 M HCl media. Experimental and theoretical study, *Int. J. Corros. Scale Inhib*., 2022, **11**, no. 3, 956–984. doi: 10.17675/2305-6894-2022-11-3-4
9. A.H. Al-Moubaraki, A.A. Ganash and S.D. Al-Malwi, Investigation of the Corrosion Behavior of Mild Steel/H_2SO_4 Systems, *Moroccan J. Chem*., 2020, **8**, 264–279. doi: 10.48317/IMIST.PRSM/morjchem-v8i1.19249
10. O. Abdellaoui, M.K. Skalli, A. Haoudi, Y. Kandri Rodi, N. Arrousse, M. Taleb, R. Ghibate and O. Senhaji, Study of the inhibition of corrosion of mild steel in a 1 M HCl solution by a new quaternary ammonium surfactant, *Moroccan J. Chem*., 2020, **9**, 44–56. doi: 10.48317/IMIST.PRSM/morjchem-v9i1.21313
11. I. Merimi, A. Bitari, Y. Kaddouri, N. Rezki, M. Mohamed, R. Touzani and B. Hammouti, Metal corrosion inhibition by triazoles: A review, *Int. J. Corros. Scale Inhib*., 2022, **11**, no. 2, 524–540. doi: 10.17675/2305-6894-2022-11-2-4

12. G. Serdaroğlu, S. Kaya and R. Touir, Eco-friendly sodium gluconate and trisodium citrate inhibitors for low carbon steel in simulated cooling water system: Theoretical study and molecular dynamic simulations, *J. Mol. Liq*., 2020, **319**, 114108. doi: 10.1016/j.molliq.2020.114108
13. M.A. Benghalia, C. Fares, A. Khadraoui, M. Hadj Meliani, I.B. Obot, A. Sorrour, M. Dmytrakh and Z. Azari, Performance evaluation of a natural and synthetic compound as corrosion inhibitors of API 5L X52 steel in hydrochloric acid media, *Moroccan J. Chem*., 2018, **6**, 51–61. doi: 10.48317/IMIST.PRSM/morjchem-v6i1.8608
14. L. Afia, R. Salghi, L. Bammou, El. Bazzi, B. Hammouti, L. Bazzi and A. Bouyanzer, Anti-corrosive properties of Argan oil on C38 steel in molar HCl solution, *J. Saudi Chem. Soc*., 2014, **18**, no. 1, 16–25. doi: 10.1016/j.jscs.2011.05.008
15. I.A. Hermoso-Diaz, A.E. Foroozan, J.P. Flores-De los Rios, L.L. Landeros-Martinez, J. Porcayo-Calderon and J.G. Gonzalez-Rodriguez, Electrochemical and quantum chemical assessment of linoleic acid as a corrosion inhibitor for carbon steel in sulfuric acid solution, *J. Mol. Struct*., 2019, **1197**, 535–546. doi: 10.1016/j.molstruc.2019.07.085
16. Y.G. Avdeev and Y.I. Kuznetsov, Physicochemical aspects of inhibition of acid corrosion of metals by unsaturated organic compounds, *Russ. Chem. Rev*., 2012, **81**, 1133–1145. doi: 10.1070/RC2012v081n12ABEH004292
17. Y.G. Avdeev, Protection of steel in solutions of mineral acids using α,β-unsaturated aldehydes, ketones, and azomethines, *Prot. Met. Phys. Chem. Surf*., 2015, **51**, 1140–1148. doi: 10.1134/S2070205115070023
18. C. Verma, M.A. Quraishi and K.Y. Rhee, Hydrophilicity and hydrophobicity consideration of organic surfactant compounds: Effect of alkyl chain length on corrosion protection, *Adv. Colloid Interface Sci*., 2022, **306**, 102723. doi: 10.1016/j.cis.2022.102723
19. N.I. Podobaev and Ya.G. Avdeev, Convective Factor in the Net Current of Iron Cathode in Sulfuric and Hydrochloric Solutions with Propargyl Alcohol and Propargyl Chloride, *Prot. Met*., 2001, **37**, no. 2, 2001, 148–150. doi: 10.1023/A:1010374005175
20. N.I. Podobaev and Ya.G. Avdeev, Specific Effects of Propargyl Alcohol and Propargyl Chloride on an Iron Electrode in Inorganic Acids, *Prot. Met*., 2000, **36**, no. 3, 251–257. doi: 10.1007/BF02758401
21. N.I. Podobaev and Ya.G. Avdeev, Temperature and Time Effects on the Acid Corrosion of Steel in the Presence of Acetylenic Inhibitor, *Prot. Met*., 2001, **37**, no. 6, 529–533. doi: 10.1023/A:1012855211234
22. Ya.G. Avdeev and Yu.I. Kuznetsov, Inhibitor protection of steel corrosion in acid solutions at high temperatures. A review. Part 2, *Int. J. Corros. Scale Inhib*., 2020, **9**, no. 2, 867–902. doi: 10.17675/2305-6894-2020-9-3-5
23. S.K. Gebauer, T.L. Psota, W.S. Harris and P.M. Kris-Etherton, n−3 fatty acid dietary recommendations and food sources to achieve essentiality and cardiovascular benefits, *Am. J. Clin. Nutr*., 2006, **83**, no. 6, 1526S–1535S. doi: 10.1093/ajcn/83.6.1526S

24. L. Guo, J. Tan, S. Kaya, S. Leng, Q. Li and F. Zhang, Multidimensional insights into the corrosion inhibition of 3,3-dithiodipropionic acid on Q235 steel in H_2SO_4 medium: A combined experimental and in silico investigation, *J. Colloid Interface Sci*., 2020, **570**, 116–124. doi: 10.1016/j.jcis.2020.03.001
25. S. Aourabi, M. Driouch, M. Sfaira, F. Mahjoubi, B. Hammouti, C. Verma, E.E. Ebenso and L. Guo, Phenolic fraction of Ammi visnaga extract as environmentally friendly antioxidant and corrosion inhibitor for mild steel in acidic medium, *J. Mol. Liq*., 2021, **323**, 114950. doi: 10.1016/j.molliq.2020.114950
26. A. Fouda, K. Shalabi and A. Idress, Thymus Vulgarise Extract as Nontoxic Corrosion Inhibitor for Copper and α-Brass in 1 M HNO_3 Solutions, *Int. J. Electrochem. Sci*., 2014, **9**, 5126.
27. I. Merimi, Y. Ouadi, K.R. Ansari, H. Oudda, B. Hammouti, M.A. Quraishi, F.F. Al-blewi, N. Rezki, M.R. Aouad and M. Messali, Adsorption and Corrosion Inhibition of Mild Steel by ((Z)-4-((2,4-dihydroxybenzylidene)amino)-5-methy-2,4 dihydro-3H-1,2,4-triazole-3-thione) in 1 M HCl: Experimental and Computational Study, *Anal. Bioanal. Electrochem*., 2017, **9**, no. 5, 640–659.
28. N. Islam and S. Kaya, *Conceptual density functional theory and its application in the chemical domain*, 2018, CRC Press.
29. A.H. Al Hamzi, H. Zarrok, A. Zarrouk, R. Salghi, B. Hammouti, S.S. Al-Deyab, M. Bouachrine, A. Amine and F. Guenoun, The Role of Acridin-9(10H)-one in the Inhibition of Carbon Steel Corrosion: Thermodynamic, Electrochemical and DFT Studies, *Int. J. Electrochem. Sci*., 2013, **8**, no. 2, 2586–2605.
30. A. Bouchtart, M. Rguiti, K. El Mouaden, A. Albourine, A. Chaouiki, R. Ralghi, L. Bazzi and A. Chetouani, Mild steel corrosion inhibition by some heteroatom organic compounds in acetic acid medium, *Moroccan J. Chem*., 2020, **8**, 982–993. doi: 10.48317/IMIST.PRSM/morjchem-v8i4.20562
31. H. Elmsellem, A. Aouniti, M. Khoutoul, A. Chetouani, B. Hammouti, N. Benchat, R. Touzani and M. Elazzouzi, Theoretical approach to the corrosion inhibition efficiency of some pyrimidine derivatives using DFT method of mild steel in HCl solution, *J. Chem. Pharm. Res*., 2014, **6**, no. 4, 1216–1224.
32. R.G. Parr, L.V. Szentpály and S. Liu, Electrophilicity index, *J. Am. Chem. Soc*., 1999, **121**, no. 9, 1922–1924. doi: 10.1021/ja983494x
33. J.L. Gázquez, A. Cedillo and A. Vela, Electrodonating and electroaccepting powers, *J. Phys. Chem. A*, 2007, **111**, no. 10, 1966–1970. doi: 10.1021/jp065459f
34. T. Koopmans, Über die Zuordnung von Wellenfunktionen und Eigenwerten zu den einzelnen Elektronen eines Atoms, *Physica*, 1934, **1**, no. 1–6, 104–113 (in German). doi: 10.1016/S0031-8914(34)90011-2
35. B. Gómez, N.V. Likhanova, M.A. Domínguez-Aguilar, R. Martínez-Palou, A. Vela and J.L. Gazquez, Quantum chemical study of the inhibitive properties of 2-pyridyl-azoles, *J. Phys. Chem. B*, 2006, **110**, no. 18, 8928–8934. doi: 10.1021/jp057143y

36. K. Barouni, A. Kassale, A. Albourine, O. Jbara, B. Hammouti and L. Bazzi, Amino acids as corrosion inhibitors for copper in nitric acid medium: Experimental and theoretical study, *J. Mater. Environ. Sci*., 2014, **5**, no. 2, 456–463.
37. L. Guo, Z.S. Safi, S. Kaya, W. Shi, B. Tüzün, N. Altunay and C. Kaya, Anticorrosive effects of some thiophene derivatives against the corrosion of iron: a computational study, *Front. Chem*., 2018, **6**, 155. doi: 10.3389/fchem.2018.00155
38. L. Guo, J. Tan, S. Kaya, S. Leng, Q. Li and F. Zhang, Multidimensional insights into the corrosion inhibition of 3,3-dithiodipropionic acid on Q235 steel in H_2SO_4 medium: A combined experimental and in silico investigation, *J. Colloid Interface Sci*., 2020, **570**, 116–124. doi: 10.1016/j.jcis.2020.03.001
39. S. Alareeqi, D. Bahamon, R.P. Nogueira and L.F. Vega, Understanding the relationship between the structural properties of three corrosion inhibitors and their surface protectiveness ability in different environments, *Appl. Surf. Sci*., 2021, **542**, 148600. doi: 10.1016/j.apsusc.2020.148600
40. D. Özbakır Işın, N. Karakuş, H. Lgaz, S. Kaya and I.M. Chung, Theoretical insights about inhibition efficiencies of some 8-Hydroxyqionoline derivatives against the corrosion of mild steel, *Mol. Simul*., 2020, **46**, no. 17, 1398–1404. doi: 10.1080/08927022.2020.1834102
41. G. Fekkar, F. Yousfi, H. Elmsellem, M. Aiboudi, M. Ramdani, I. Abdel-Rahman, B. Hammouti and L. Bouyazza, Eco-friendly *Chamaerops humilis* L. fruit extract corrosion inhibitor for mild steel in 1 M HCl, *Int. J. Corros. Scale Inhib*., 2020, **9**, no. 2, 446–459. doi: 10.17675/2305-6894-2020-9-2-4
42. A.A. EL Hassani, Z. El Adnani, A.T. Benjelloun, M. Sfaira, M. Benzakour, M. Mcharfi, B. Hammouti and K.M. Emran, DFT theoretical study of 5-(4-R-phenyl)-1*H*-tetrazole (R=H; OCH_3; CH_3; Cl) as corrosion inhibitors for mild steel in hydrochloric acid, *Met. Mater. Int*., 2020, **26**, no. 11, 1725–1733. doi: 10.1007/s12540-019-00381-5
43. A.S. Fouda, K. Shalabi and A.A. Idress, Thymus vulgarise extract as nontoxic corrosion inhibitor for copper and α-brass in 1 M HNO_3 solutions, *Int. J. Electrochem. Sci*., 2014, **9**, no. 9, 5126–5154.
44. M. Bouklah, B. Hammouti, M. Lagrenee and F. Bentiss, Thermodynamic properties of 2,5-bis (4-methoxyphenyl)-1,3,4-oxadiazole as a corrosion inhibitor for mild steel in normal sulfuric acid medium, *Corros. Sci*., 2006, **48**, no. 9, 2831–2842. doi: 10.1016/j.corsci.2005.08.019
45. O. Olivares-Xometl, N.V. Likhanova, M.A. Domínguez-Aguilar, E. Arce, H. Dorantes and P. Arellanes-Lozada, Synthesis and corrosion inhibition of α-amino acids alkylamides for mild steel in acidic environment, *Mater. Chem. Phys*., 2008, **110**, no. 2–3, 344–351. doi: 10.1016/j.matchemphys.2008.02.010
46. I.N. Putilova, S.A. Balezin and V.P. Barannik, *Metallic corrosion inhibitors*, 1960, Pergamon Press.

47. A. Zarrouk, B. Hammouti, T. Lakhlifi, M. Traisnel, H. Vezin and F. Bentiss, New 1*H*-pyrrole-2,5-dione derivatives as efficient organic inhibitors of carbon steel corrosion in hydrochloric acid medium: electrochemical, XPS and DFT studies, *Corros. Sci*., 2015, **90**, 572–584. doi: 10.1016/j.corsci.2014.10.052
48. B.A. Abd-EI-Nabey, E. Khamis, M.S. Ramadan and A. El-Gindy, Application of the kinetic-thermodynamic model for inhibition of acid corrosion of steel by inhibitors containing sulfur and nitrogen, *Corrosion*, 1996, **52**, no. 09, 671–679. doi: 10.5006/1.3292157
49. A. Chetouani, B. Hammouti, A. Aouniti, N. Benchat and T. Benhadda, New synthesised pyridazine derivatives as effective inhibitors for the corrosion of pure iron in HCl medium, *Prog. Org. Coat*., 2002, **45**, no. 4, 373–378. doi: 10.1016/S0300-9440(02)00123-6
50. J.O. Bockris and A.K.N. Reddy, *Modern Electrochemistry*, 1970, Springer US, Boston. doi: 10.1007/978-1-4615-7467-5
51. L.I. Antropov, *Theoritical Electrochemistry*, Mir, Moscow, (1972).
52. J. Ćwiek, Hydrogen degradation of high-strength steels, *J. Achiev. Mater. Manuf. Eng*., 2009, **37**, no. 2, 193–212.
53. M. Manssouri, Y. El Ouadi, M. Znini, J. Costa, A. Bouyanzer, J-M. Desjobert and L. Majidi, Adsorption proprieties and inhibition of mild steel corrosion in HCl solution by the essential oil from fruit of Moroccan *Ammodaucus leucotrichus*, *J. Mater. Environ. Sci*., 2015, **6**, 631–646.
54. I. Ghazi, S. Jorio, S. Mostapha, R. Fdil and H. El attari, Experimental and theoretical studies on corrosion inhibitory action of *Peganum harmala* (L.) seeds extract on carbon steel in 1 M HCl, *Moroccan J. Chem*., 2021, **9**, 542–563. doi: 10.48317/IMIST.PRSM/morjchem-v9i3.22928
55. F. El Hajjaji, H. Greche, M. Taleb, A. Chetouani, A. Aouniti and B. Hammouti, Application of essential oil of thyme vulgaris as green corrosion inhibitor for mild steel in 1 M HCl, *J. Mater. Environ. Sci*., 2016, **7**, no. 2, 567–578.
56. M. Goyal, S. Kumar, L. Guo, S.H. Alrefaee and C. Verma, Influence of Ring Size on Corrosion Inhibition Potential of Environmental Sustainable Cycloalkyltriphenylphosphonium based Ionic Liquids: Computational and Experimental Demonstrations, *J. Taiwan Inst. Chem. Eng*., 2021, **123**, 21–33. doi: 10.1016/j.jtice.2021.05.026
57. A. Zarrouk, A. Chelfi, A. Dafali, B. Hammouti, S.S. Al-Deyab, I. Warad, N. Benchat and M. Zertoubi, Comparative Study of new Pyridazine Derivatives Towards Corrosion of Copper in Nitric Acid: Part-1, *Int. J. Electrochem. Sci*., 2010, **5**, 696–705.
58. S.A. Umoren, M.M. Solomon, I.B. Obot and R.K. Suleiman, Comparative studies on the corrosion inhibition efficacy of ethanolic extracts of date palm leaves and seeds on carbon steel corrosion in 15% HCl solution, *J. Adhes. Sci. Technol*., 2018, **32**, no. 17, 1934–1951. doi: 10.1080/01694243.2018.1455797

59. A. Zouitini, Y. Kandri Rodi, Y. Ouzidan, F. Ouzzani Chahdi, M. Mokhtari, I. Abdel-Rahman, E.M. Essassi, A. Aouniti, B. Hammouti and H. Elmsellem, Corrosion inhibition studies of new synthesized 1,4-dioctyl-6-methyl-1,4-dihydroquinoxaline-2,3-dione on mild steel in 1.0 M HCl solution using gravimetric and electrochemical techniques supported by theoretical DFT calculations, *Int. J. Corros. Scale Inhib*., 2019, **8**, no. 2, 225–240. doi: 10.17675/2305-6894-2019-8-2-5
60. C. Verma, E.E. Ebenso and M.A. Quraishi, Corrosion inhibitors for ferrous and non-ferrous metals and alloys in ionic sodium chloride solutions: A review, *J. Mol. Liq*., 2017, **248**, 927–942. doi: 10.1016/j.molliq.2017.10.094
61. A.O. Yüce and G. Kardaş, Adsorption and inhibition effect of 2-thiohydantoin on mild steel corrosion in 0.1 M HCl, *Corros. Sci*., 2012, **58**, 86–94. doi: 10.1016/j.corsci.2012.01.013
62. S. Kaya and C. Kaya, A new method for calculation of molecular hardness: a theoretical study, *Comput. Theor. Chem*., 2015, **1060**, 66–70. doi: 10.1016/j.comptc.2015.03.004
63. S. Kaya and C. Kaya, A new equation for calculation of chemical hardness of groups and molecules, *Mol. Phys*., 2015, **113**, no. 11, 1311–1319. doi: 10.1080/00268976.2014.991771
64. S. Kaya and C. Kaya, A simple method for the calculation of lattice energies of inorganic ionic crystals based on the chemical hardness, *Inorg. Chem*., 2015, **54**, no. 17, 8207–8213. doi: 10.1021/acs.inorgchem.5b00383
65. P.K. Chattaraj, S. Nath and B. Maiti, *Reactivity descriptors*, 2003, Marcel Dekker: New York, 295–322.
66. L. von Szentpály, S. Kaya and N. Karakuş, Why and when is electrophilicity minimized? New theorems and guiding rules, *J. Phys. Chem. A*, 2020, **124**, no. 51, 10897–10908. doi: 10.1021/acs.jpca.0c08196
67. S. Kaya and C. Kaya, A new equation based on ionization energies and electron affinities of atoms for calculating of group electronegativity, *Comput. Theor. Chem*., 2015, **1052**, 42–46. doi: 10.1016/j.comptc.2014.11.017
68. D.B. Tripathy, M. Murmu, P. Banerjee and M.A. Quraishi, Palmitic acid based environmentally benign corrosion inhibiting formulation useful during acid cleansing process in MSF desalination plants, *Desalination*, 2019, **472**, 114128. doi: 10.1016/j.desal.2019.114128

♦ ♦ ♦